One-Dimensional and Two-Dimensional Quantum Systems on Carbon Nanotube Bundles

J. V. Pearce,[1,2] M. A. Adams,[3] O. E. Vilches,[4] M. R. Johnson,[1] and H. R. Glyde[2]

[1]*Institut Laue-Langevin, BP 156, 38042 Grenoble, France*
[2]*Department of Physics and Astronomy, University of Delaware, Delaware 19716-2570, USA*
[3]*ISIS Facility, Rutherford Appleton Laboratory, Didcot, OX11 0QX, United Kingdom*
[4]*Department of Physics, University of Washington, Seattle, Washington 98195-1560, USA*

(Received 10 May 2005; published 24 October 2005)

We report the first measurement of the structure of ^{4}He atoms adsorbed on bundles of single-walled carbon nanotubes. Neutron diffraction techniques and nanotube samples closed at the end were used. At low coverage, ^{4}He forms a 1D, single line lattice along the grooves between two nanotubes on the surface of the nanotube bundles. As coverage is increased, additional lines of 1D lattices form along the grooves. This is followed by an incommensurate, 2D monolayer covering the whole nanotube bundle surface. The lattice constants of these 1D and 2D systems are largely independent of filling once a single 1D line is formed. No occupation of the interstitial channels between nanotubes is observed in the present sample.

DOI: 10.1103/PhysRevLett.95.185302 PACS numbers: 67.80.Cx, 61.12.Ex, 61.12.Ld, 61.46.+w

Helium and hydrogen adsorbed on and in nanotubes are predicted to form exotic quantum states of matter [1,2]. For example, calculations suggest that ^{4}He and H_2 form one-dimensional (1D) systems when confined inside nanotubes or along the grooves between two adjacent nanotubes on the exterior surface of a nanotube bundle [1,3–6]. Specifically, along the grooves ^{4}He is predicted to form a single 1D line at low coverages and subsequently three 1D lines, denoted the ''three-line'' phase, at higher coverages. At still higher dosing, ^{4}He and H_2 are predicted to form a 2D incommensurate monolayer on the surface of nanotube bundles [1,7]. Helium dimers are stabilized by 4 orders of magnitude in energy inside carbon nanotubes [8,9]. These simple 1D, 2D and molecular states are excellent test beds for fundamental mesoscopic quantum physics and statistical mechanics in reduced dimension [2,7,10]. However, none of these structures have been observed directly.

Experimentally, specific heat measurements of ^{4}He on single-walled carbon nanotube (SWNT) bundles show 1D character at low coverages and 2D character near monolayer coverages on larger nanotube bundles [11]. Thermal desorption, volumetric adsorption isotherms and AC heat capacity measurements have been used to deduce adsorption energies [12–15]. They suggest that there are two absorption sites, a high binding energy site (associated with ^{4}He in interstitial channels or groove sites) and a lower energy, graphene-like site (associated with ^{4}He on the nanotube bundle surface) [1]. Recent neutron diffraction and thermodynamic measurements of D_2 and heavier gases, e.g., Ar, O_2, CO_2, and CH_4, adsorbed on SWNTs provide much information on structure and binding energies [16–18]. For bundles having 1.7 nm intertube spacing, the heavier gases are adsorbed initially in 1D structures in the grooves (G) on the bundle surfaces and in imperfect interstitial channels (IC's) between nanotubes [19,20]. At higher coverages, quasi-2D layers form on the bundle surfaces.

We report the first measurements of the structure of ^{4}He adsorbed on closed-end, SWNT bundles. As a function of dosing, our measurements show that ^{4}He forms first as 1D line lattices. The 1D structure is observed in a coverage range corresponding to completion of a single 1D line and of three 1D lines along the grooves on the bundle surfaces. Our measurements cannot distinguish between the structure of a single 1D line and a number of 1D lines. Our data and simulations show no occupation of IC spaces between nanotubes in the present 1.4 nm intertube spacing bundles. At higher dosing, ^{4}He forms a complete 2D incommensurate monolayer lattice over the surface of the nanotube bundle thus exhibiting 1D to 2D crossover. We have performed simulations that lead to the 1D line, the ''three-line phase,'' and the incommensurate monolayer depicted schematically in Fig. 1. The simulated diffraction from these phases also show 1D and 2D components. The observed 1D to 2D crossover agrees with predictions [1,21] and specific heat measurements [11,22], but predicted IC site occupation [1,21] is not observed. These direct measurements of structure versus dosing, supported by numerical modeling, open the door to reliable creation of 1D and 2D highly quantum systems and to 1D to 2D crossover at well-defined ^{4}He coverages on nanotubes.

SWNTs are sheets of carbon atoms (graphene sheets) rolled into a seamless cylinder. The cylinder is typically

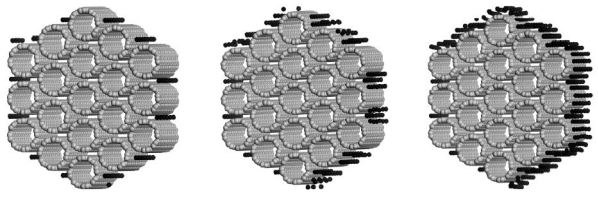

FIG. 1. Structure of ^{4}He atoms adsorbed on a SWNT bundle. Left: 1D chains. Middle: ''three-line'' phase. Right: 1 monolayer coverage.

1–2 nanometers in diameter and several thousand nanometers long forming a nearly 1D system. SWNTs are one of a class of exotic carbon nanostructures that includes the Buckminsterfullerenes and carbon onions [23]. The SWNTs typically self assemble into bundles or ropes containing 50 or more tubes. The present 2.7 g closed-end Bucky Pearls™ SWNT sample was purchased from Carbon Nanotechnologies Inc. (Houston, Texas) as were the HiPco™ bundles used by Wilson and Vilches [22]. The manufacture of these two samples is similar [24]. The sample was outgassed at 500 K in vacuum for three days and thereafter mounted (in a ^{4}He atmosphere) in an aluminum sample cell in a standard "orange" cryostat for cooling to 2.5 K. Adsorption isotherms were measured at temperatures between 5 and 15 K prior to the neutron measurements for guidance with desired coverages and for comparison with previous isotherm measurements [15,22].

Our diffraction measurements were performed on the D20 diffractometer at the Institut Laue-Langevin, Grenoble, with an incident neutron wavelength of $\lambda = 2.414$ Å and a scattering vector range $0.2 < Q < 5.0$ Å^{-1}. Here, $Q = (4\pi/\lambda)\sin\theta$, where 2θ is the scattering angle. ^{4}He was condensed onto the nanotubes at a temperature of 15 K, and allowed to equilibrate at this temperature for 30 minutes. The temperature was then reduced slowly to 2.5 K. Neutron diffraction spectra were measured for 18 ^{4}He doses between 1.9 and 222 cm^3/g at STP. A monolayer on the bundle surface is complete at a coverage of ~220 cm^3/g or 4.0 wt % of ^{4}He.

Figure 2 shows the total scattered intensity, $S(Q)$, from the cell containing the SWNTs without ^{4}He. There is a single broad peak at $Q \simeq 0.55$ Å^{-1} arising from the triangular structure of the SWNTs within the bundles, the first order (10) bundle lattice peak. This gives an average spacing between the nanotubes of 1.4 ± 0.2 nm, the same as observed in HiPco SWNTs by x-ray diffraction [24]. The broad (10) peak and the absence of higher order peaks indicates, among other possibilities, a distribution of nanotube diameters which leads to a distribution of tube spacings and introduces packing defects both of which broaden $S(Q)$. The degree of crystallinity of the bundle is comparable to that of the "Montpellier" sample [25] but not so good as the samples used subsequently by Rols *et al.* in neutron diffraction experiments [16,26] which show a narrower (10) peak and higher order diffraction peaks (and a lattice spacing of 1.7 ± 0.1 nm). The degree of crystallinity within the bundles is not expected to have an impact on the adsorption on the bundle surface. However, the distribution of nanotube diameters is expected to lead to a distribution of lattice spacings of the ^{4}He on the surface as discussed below.

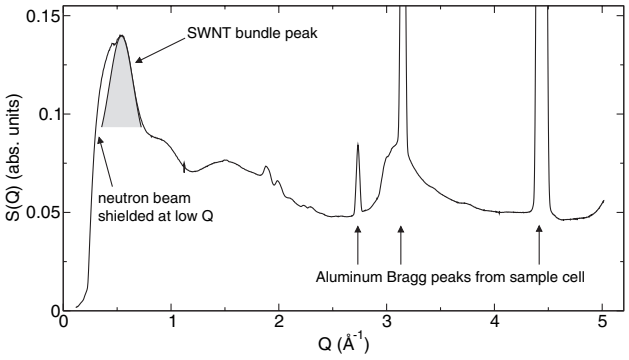

FIG. 2. Neutron diffraction intensity, $S(Q)$, from the bare SWNTs. The (10) bundle lattice peak is seen at $Q \simeq 0.55$ Å^{-1} and is highlighted by the shaded peak to guide the eye. The rising intensity expected at small angle scattering (at low Q) is not seen because the neutron beam at small scattering angle was blocked to avoid damage to the detectors.

Figure 3 shows the net scattering intensity, $S(Q)$, from ^{4}He on the nanotubes for ^{4}He coverages ranging from 1.9 cm^3/g to 222 cm^3/g. In Fig. 3 we see net negative intensity for $Q < 1.5$ Å^{-1} and net positive scattering for $Q > 1.5$ Å^{-1} (except at $Q \sim 3.2$ Å^{-1}). When the nanotubes are bare, there is substantial scattering from the structure of the nanotube surfaces, except at very low Q where the nanotubes look structureless. The scattering from this structure is reduced when ^{4}He is deposited on the surface. This leads to net negative intensity for $Q < 1.5$ Å^{-1} (and a second order contribution at $Q \sim 3.2$ Å^{-1}) which is proportional to the ^{4}He coverage. This negative intensity is observed universally for all gases on nanotubes investigated to date [17,27]. The intensity at $Q = 4.4$ Å^{-1} has been removed because there is some residue from subtraction of a large Bragg peak from the aluminum sample cell.

The net positive intensity in the range $1.5 < Q < 2.5$ Å^{-1} and $3 < Q < 4.5$ Å^{-1} are the first and second

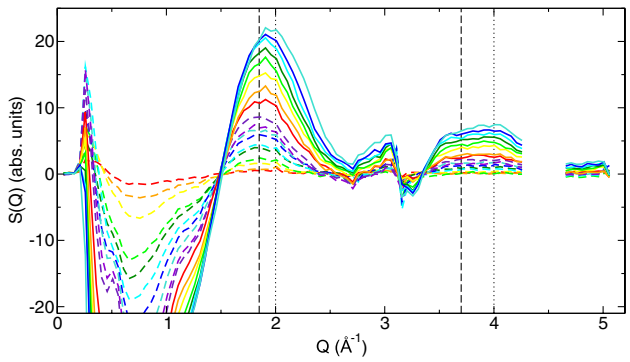

FIG. 3 (color online). Net neutron diffraction intensity from ^{4}He on SWNTs after subtraction of the bare SWNT intensity. The weakest intensity corresponds to the lowest ^{4}He coverage, 1.9 cm^3/g, and the strongest corresponds to the highest coverage, 222 cm^3/g. Dashed lines mark the wave vectors Q_1 and $2Q_1$ at which the first and second order Bragg peak intensities for a 1D lattice of ^{4}He are expected. The dotted lines mark the wave vectors Q_2 and $2Q_2$ where the corresponding intensities for a 2D monolayer are expected.

order Bragg reflections, respectively, from the ^{4}He on the nanotubes. Specifically, the first and second order reflections from the 1D single line and "three-line" phases of ^{4}He with lattice spacing a_1 are expected at $Q_1 = 2\pi/a_1$ and $2Q_1$, respectively. The first and second order reflections for a triangular 2D lattice with spacing a_2 are expected at $Q_2 = 4\pi/(a_2\sqrt{3})$ and at $2Q_2$ respectively. The values of Q_1 and $2Q_1$ and of Q_2 and $2Q_2$ for the values of a_1 and a_2 that we find eventually below are shown in Fig. 3.

To assist interpretation, we simulated the diffraction using the CERIUS2^{TM} [28] molecular modeling programs written by Accelrys. The nanotubes were represented by a single bundle of 19 tubes in an "8-8 armchair" configuration. This bundle has the cross section shown in Fig. 1. The He-carbon and He-He interactions were represented by Lennard-Jones (LJ) potentials. Thermodynamic and isotherm measurements [15,22] indicate that filling of the higher binding energy sites expected for a 1D line and three 1D lines in the G sites are complete at approximately 18 and 55 cm^3/g (0.33 wt % and 1.0 wt % of ^{4}He). The filling of lower energy sites expected for monolayer sites is complete at 220 cm^3/g. The configuration of the ^{4}He atoms on the nanotubes at these three fillings was determined by minimizing the classical energy of the ^{4}He and nanotube system. This energy minimization led to the 1D line, the "three-line," and the 2D monolayer phases displayed in Fig. 1. No occupation of IC sites was found; for this sample there is not sufficient space between the tubes. The 1D line is commensurate so that the 1D lattice spacing a_1 is set by the nanotube structure—as found in other simulations [2]. The 2D monolayer was found to be incommensurate. To obtain the observed spacing a_2 we increased the LJ hard core parameter to $\sigma = 3.96$ Å to simulate the role of zero point energy not included in our classical energy minimization.

Figure 4(b) shows the simulated net diffraction from the ^{4}He in this model in the three configurations shown in Fig. 1. This simulated diffraction shows intensity from 1D lines and from 2D monolayers. The simulated peaks are sharper than those observed in Fig. 4(a) since a single bundle with identical diameter nanotubes is simulated.

We were able to reproduce the broad observed peaks shown in Fig. 4(a) for 1D lines by (1) introducing a distribution of line lattice spacings, (2) introducing defect regions in a given line, and (3) using finite length lines. A distribution of lattice spacings is expected both from the distribution of nanotube diameters noted above and from variations of the nanotube chirality [2,16]. Broad, Gaussian diffraction peaks arise when these inhomogeneities are incorporated.

To display the crossover from 1D to 2D adsorption with increasing filling, we present the data in Fig. 5 as the net $S(Q)$ per unit of ^{4}He adsorbed for fillings between completion of three 1D lines (55 cm^3/g) and completion of a monolayer (222 cm^3/g). $S(Q)$ for Q values in the first order reflection region are shown. At 55 cm^3/g, $S(Q)$ peaks at $Q = 1.60$ Å^{-1} while at 222 cm^3/g $S(Q)$ peaks at $Q = 1.95$ Å^{-1}. There is a clear difference in the shape of $S(Q)$ arising from 1D and 2D structures.

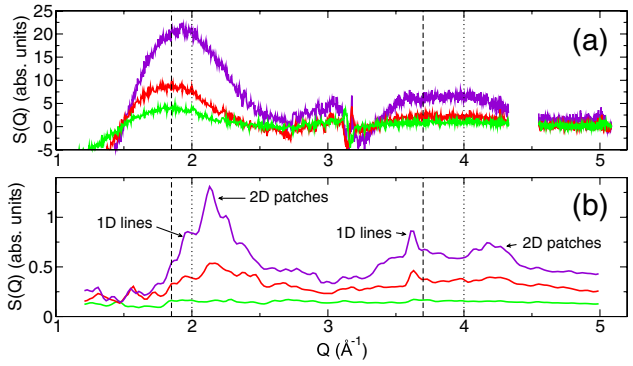

FIG. 4 (color online). Observed (a) and calculated (b) net neutron diffraction intensity, $S(Q)$, from ^{4}He on SWNTs. The dashed lines are Q_1 and $2Q_1$, the dotted lines Q_2 and $2Q_2$ as defined in Fig. 3. The observed intensities $S(Q)$ are at ^{4}He coverages of 20.5 cm^3/g (the curve that starts furthest left, green online), 69.3 cm^3/g (middle curve, red online) and 222 cm^3/g (top curve, purple online). The calculated $S(Q)$ are at coverages corresponding to completion of a linear chain in the grooves at ~18 cm^3/g (bottom, green online), of three linear chains at ~55 cm^3/g (middle, red online), and of a monolayer at ~220 cm^3/g (top, purple online) (see Fig. 1).

To determine the values of a_1 and a_2 explicitly, the observed 1D line and 2D monolayer first order reflection intensities shown in Fig. 3 were each represented by a Gaussian centered at Q_1 and Q_2, respectively. Fits were made to the data at each filling with Q_1 and Q_2 and the weight of the Gaussians taken as free fitting parameters (see inset of Fig. 6). The width of the Gaussians (arising from the nanotube diameter distribution) was held independent of filling. The resulting values of a_1 and a_2 and the corresponding 1D and 2D intensities obtained from the fits are shown in Fig. 6. This shows that a_1 increases very

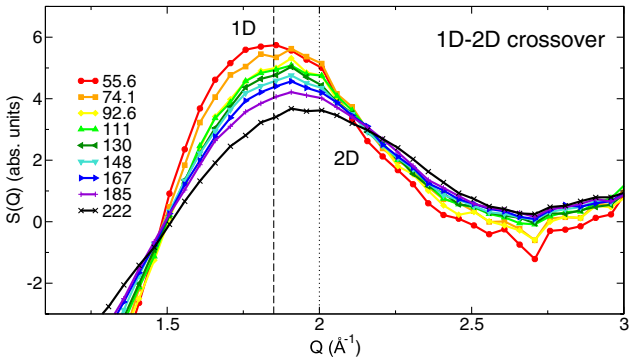

FIG. 5 (color online). Net $S(Q)$ from adsorbed ^{4}He divided by the amount of ^{4}He adsorbed for coverages between filled "three-lines" (1D regime) and the nearly complete monolayer (2D regime). The result is a clear visualization of the change of *form* of the line shape as the structure per ^{4}He adsorbed changes from 1D (55.6 cm^3/g) to 2D (222 cm^3/g).

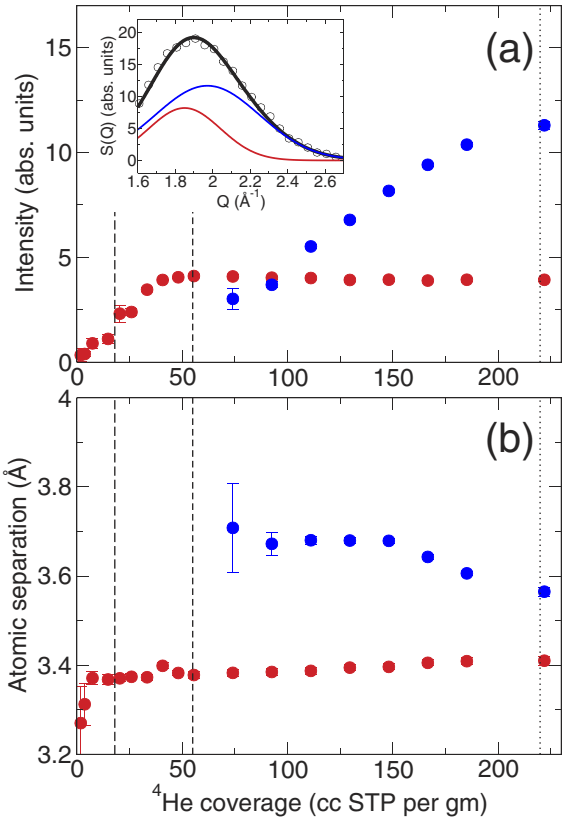

FIG. 6 (color online). (a) Intensity in the first order Bragg peak region of $S(Q)$ arising from the 1D lattice (dots starting at zero, red online) and from the 2D lattice (dots starting at 75, blue online) versus coverage. (b) The 1D and 2D lattice spacings versus coverage. The observed $S(Q)$ is expressed as the sum of two Gaussian functions, one representing the 1D (bottom left, red online) and the other the 2D (top, blue online) diffracted peaks. The intensity and lattice parameter in each component is found by fitting the magnitude and center in Q of the Gaussians to the data. Coverages of 1 line, 3 lines, and 1 monolayer are indicated by long dashed, short dashed, and dotted lines.

slightly with coverage, giving a nearly constant $a_1 = 3.40 \pm 0.02$ Å, and a_2 is very slightly compressed as a function of coverage, with $a_2 = 3.70 \pm 0.03$ Å at low coverage, becoming $a_2 = 3.63 \pm 0.03$ Å at monolayer completion.

In summary, we have observed the structure of ^{4}He on the surface of nanotube bundles using neutron diffraction. ^{4}He forms 1D line lattices at low coverages, up to fillings consistent with completion of three 1D lines along the groove sites (55 cm^3/g). At higher fillings, ^{4}He forms a 2D triangular lattice on the bundle surface with monolayer completion at 220 cm^3/g. The 1D lattice spacing ($a_1 = 3.40 \pm 0.02$ Å) appears to increase very slightly with increasing coverage which is not understood. The 2D lattice spacing decreases slightly with filling indicating very slight compression of the 2D lattice with increasing coverage. No occupation of the interchannel spaces between nanotubes is indicated for the present intertube spacing of 1.4 ± 0.2 nm. The present results show that 1D and 2D quantum systems at nearly constant lattice parameter and 1D–2D crossover can be reliably created using ^{4}He on commercially available nanotubes.

We are indebted to Michel Bienfait for lending us his sample stick and cell. We thank Thomas Hansen, Paul Henry, and Jacques Torregrossa, Institut Laue-Langevin, for technical assistance and John Larese, Eckhard Krotscheck, and Hans Lauter for valuable discussions. Partial support of this work by NSF DMR 0245423 and DMR 0115663 (O. E. V.), and DOE DE-FG02-03ER46038 (H. R. G.) is gratefully acknowledged.

[1] M. M. Calbi *et al.*, Rev. Mod. Phys. **73**, 857 (2001).
[2] M. Aichinger *et al.*, Phys. Rev. B **70**, 155412 (2004).
[3] J. Boronat, M. C. Gordillo, and J. Casulleras, J. Low Temp. Phys. **126**, 199 (2002).
[4] E. Krotscheck and M. D. Miller, Phys. Rev. B **60**, 13 038 (1999).
[5] M. Boninsegni and S. Moroni, J. Low Temp. Phys. **118**, 1 (2000).
[6] M. C. Gordillo, J. Boronat, and J. Casulleras, Phys. Rev. Lett. **85**, 2348 (2000).
[7] A. Firlej and B. Kuchta, Colloids Surf. A **241**, 149 (2004).
[8] Y. Vranješ, Z. Antunovic, and S. Kilić, Physica (Amsterdam) **329B**, 276 (2003).
[9] Y. Vranješ, Z. Antunovic, and S. Kilić, Physica (Amsterdam) **349B**, 408 (2004).
[10] F. Ancilotto *et al.*, Phys. Rev. B **70**, 165422 (2004).
[11] J. C. Lasjaunias *et al.*, Phys. Rev. Lett. **91**, 025901 (2003).
[12] W. Teizer *et al.*, Phys. Rev. Lett. **82**, 5305 (1999).
[13] W. Teizer *et al.*, Phys. Rev. Lett. **84**, 1844(E) (2000).
[14] R. B. Hallock and Y. H. Kahng, J. Low Temp. Phys. **134**, 21 (2004).
[15] T. Wilson and O. E. Vilches, Physica (Amsterdam) **329B**, 278 (2003).
[16] S. Rols *et al.*, Phys. Rev. B **71**, 155411 (2005).
[17] M. Bienfait *et al.*, Phys. Rev. B **70**, 035410 (2004).
[18] S. Talapatra and A. D. Migone, Phys. Rev. Lett. **87**, 206106 (2001).
[19] W. Shi and J. K. Johnson, Phys. Rev. Lett. **91**, 015504 (2003).
[20] V. Krungleviciute *et al.*, Nano Lett. **4**, 1133 (2004).
[21] S. M. Gatica *et al.*, J. Low Temp. Phys. **120**, 337 (2000).
[22] T. Wilson and O. E. Vilches, Fiz. Nizk. Temp. **29**, 975 (2003) [Low Temp. Phys. **29**, 732 (2003)].
[23] M. Terrones and H. Terrones, Phil. Trans. R. Soc. A **361**, 2789 (2003).
[24] I. W. Chiang *et al.*, J. Phys. Chem. B **105**, 8297 (2001).
[25] S. Rols *et al.*, Eur. Phys. J. B **10**, 263 (1999).
[26] S. Rols *et al.*, Phys. Rev. Lett. **85**, 5222 (2000).
[27] M. R. Johnson *et al.*, Chem. Phys. **293**, 217 (2003).
[28] Available from http://www.accelrys.com.